Chemical Science

ROYAL SOCIETY OF CHEMISTRY

EDGE ARTICLE

View Article Online
View Journal | View Issue

Cite this: *Chem. Sci.*, 2024, **15**, 230

All publication charges for this article have been paid for by the Royal Society of Chemistry

Received 28th September 2023
Accepted 28th November 2023

DOI: 10.1039/d3sc05098j

rsc.li/chemical-science

Interface regulation of the Zn anode by using a low concentration electrolyte additive for aqueous Zn batteries†

Kuo Wang,‡[a] Qianrui Li,‡[a] Guoli Zhang,[a] Shuo Li,[a] Tong Qiu,[a] Xiao-Xia Liu [abc] and Xiaoqi Sun *[ab]

The Zn metal anode in aqueous Zn batteries faces a number of challenges including instable deposition and corrosion issues. Here, we present an interface environment regulation for a Zn electrode with a low concentration electrolyte additive of 0.1 m 3-aminobenzenesulfonic acid (ASA). ASA prefers to adsorb on the Zn surface over water and creates an ASA-rich interface. It further enters the Zn^{2+} solvation sheath locally, which shifts the lowest unoccupied molecular orbital from solvated water to ASA. The hydrogen evolution reaction from solvated water reduction is inhibited, and the reduction of solvated ASA generates a stable solid-electrolyte interphase composed of the ion conductor ZnS covered by organic–inorganic mixed components. With the resulting homogenized Zn deposition, continuous Zn stripping in symmetric cells reaches 99.7% depth of discharge (DOD) at a current density of 2 mA cm^{-2}, whereas cell short-circuit takes place at 11.4% DOD in the ASA free $ZnSO_4$ electrolyte. The repeated stripping/plating also realizes 1100 h cycle life at 2 mA cm^{-2}, and a 99.54% stabilized coulombic efficiency is obtained for 500 cycles at 10 mA cm^{-2}.

Introduction

Rechargeable aqueous zinc batteries have received great attention recently for their outstanding benefits of intrinsic high safety and low cost.[1–8] The metallic Zn anode provides high theoretical specific capacity (820 mA h g^{-1} or 5855 mA h cm^{-2}) and low redox potential (−0.76 V *vs.* S.H.E.). However, it also faces a number of challenges such as Zn dendrite formation and corrosion reactions.[9–20] They seriously hinder the coulombic efficiency and cycle life of zinc batteries. Numerous strategies have been proposed to address the issues with Zn metal anodes. Among them, electrolyte additive engineering is of great importance for its simplicity and good efficiency. Additives can alter the Zn^{2+} solvation sheath, modify the hydrogen bonding network and induce solid-electrolyte interphase (SEI) formation, which helps to regulate Zn deposition behavior and inhibit side reactions such as the hydrogen evolution reaction (HER). Dimethyl carbonate (DMC),[21] 1,2-dimethoxyethane (DME),[22] and propylene carbonate (PC)[23] additives are good examples to effectively enhance the stability of Zn anodes. Nevertheless, an important requirement for an additive is a relatively low concentration, in order to not affect the cost, safety, and the excellent physical properties such as viscosity and ionic conductivity of aqueous electrolytes.

Since any plating/stripping or side reactions take place at the interface between the Zn electrode and electrolyte, molecules that are able to replace water at the Zn interface would create a locally additive-rich environment and provide an effective regulation of Zn anode behavior even with low overall content. The bulk electrolyte properties are retained. Following this consideration, we herein apply 3-aminobenzene sulfonic acid (ASA) as the additive in the 2 m (mol kg^{-1}) $ZnSO_4$ aqueous electrolyte. A low optimized concentration of 0.1 m is identified. Theoretical calculations and experimental analysis confirm that ASA preferentially adsorbs on the Zn surface and participates in the Zn^{2+} inner solvation sheath at the interface. In comparison to the reduction of solvated water in the typical $Zn(H_2O)_6^{2+}$ solvation structure and the resulting HER, the lowest unoccupied molecular orbitals (LUMOs) dominate on ASA after it enters Zn^{2+} solvation shells. This not only inhibits the HER, but also generates a gradient SEI on the Zn electrode. Therefore, the cycle life of a Zn//Zn symmetric cell extends from 110 h to 1100 h at 2 mA cm^{-2} with the help of an ASA additive. The ASA containing electrolyte also provides a stabilized coulombic efficiency of 99.45% for 500 cycles at 10 mA cm^{-2}.

[a]*Department of Chemistry, Northeastern University, Shenyang 110819, China. E-mail: sunxiaoqi@mail.neu.edu.cn*

[b]*National Frontiers Science Center for Industrial Intelligence and Systems Optimization, Northeastern University, 3-11 Wenhua Road, Shenyang, 110819, China*

[c]*Key Laboratory of Data Analytics and Optimization for Smart Industry, Ministry of Education, Northeastern University, China*

† Electronic supplementary information (ESI) available. See DOI: https://doi.org/10.1039/d3sc05098j

‡ These authors contributed equally to this work.

Results and discussion

The effect of the ASA electrolyte additive on the electrochemical performance of the Zn electrode is first studied. Repeated stripping/plating of Zn is evaluated in symmetric cells, with the 2 m $ZnSO_4$ solution used as the benchmark electrolyte. Fig. 1a shows the lifespans at a current density of 2 mA cm^{-2} and capacity of 2 mA h cm^{-2}. The cell with the neat $ZnSO_4$ electrolyte (labeled as no-ASA) experiences short circuit after 110 h. With the addition of 0.01 m and 0.05 m ASA (labeled as 0.01-ASA and 0.05-ASA, respectively), the cycle life extends to 793 h and 854 h, respectively. A long-term cycling stability over 1100 h is finally achieved with the electrolyte containing the 0.1 m ASA additive (labeled as 0.1-ASA). Further increasing the ASA concentration to 0.15 m leads to precipitation in the solution (Fig. S1†), and 0.1 m is identified as the optimal additive concentration. It is worth noting that a low addition of 0.1 m ASA has almost no effect on the ionic conductivity of the electrolyte (Fig. S2†). Fig. S3† compares the voltage curves of Zn stripping/plating with the neat $ZnSO_4$ and 0.1-ASA electrolytes at current densities from 1 mA cm^{-2} to 20 mA cm^{-2} and a capacity of 2 mA h cm^{-2}. The cell short circuits at 10 mA cm^{-2} in $ZnSO_4$. In contrast, the cell with the 0.1-ASA electrolyte functions properly at all current densities. Repeated stripping/plating in symmetric cells is further carried out at higher current densities of 5 mA cm^{-2} and 10 mA cm^{-2} (Fig. 1b and c). The cells with 0.1-ASA stably function for over 600 h and 400 h, respectively, whereas cell short-circuits take place at 48 h and 50 h in the neat $ZnSO_4$ electrolyte. Symmetric cells are further assembled with thin Zn electrodes (~20 μm), and stripping/plating is carried out at 2 mA cm^{-2} and 4 mA h cm^{-2}, which corresponds to a 35% depth of discharge (DOD, Fig. 1d). In $ZnSO_4$, the voltage of the cell fluctuates greatly from the 3rd cycle. By contrast, an extended cycle life of 200 h is achieved in the 0.1-ASA electrolyte.

Single stripping/plating is then carried out at different current densities in symmetric cells (Fig. 1e–h). With the $ZnSO_4$ electrolyte, cell short circuits take place after the capacity reaches 11.06 mA h cm^{-2}, 12.55 mA h cm^{-2} and 12.30 mA h cm^{-2} with a current density of 2 mA cm^{-2}, 5 mA cm^{-2} and 10 mA cm^{-2}, respectively. They correspond to the DOD of 11.4%, 12.9% and 12.7% of the stripping electrode. With the introduction of 0.1 m ASA in the electrolyte, in contrast, much higher DOD values of 99.7%, 58.3% and 34.3% are achieved at the corresponding current densities. Notably, the voltage increase

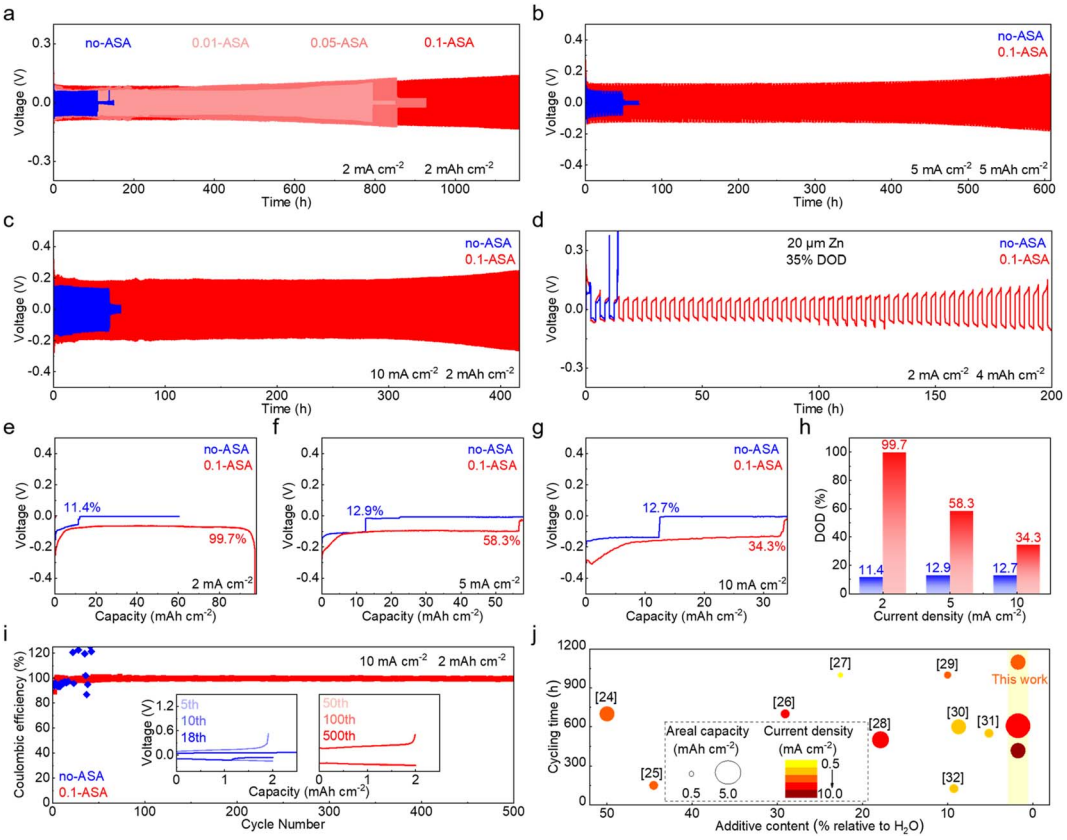

Fig. 1 (a) Long-term cycling of Zn//Zn symmetric cells in the $ZnSO_4$ electrolytes without and with different concentrations of the ASA additive at 2 mA cm^{-2} and 2 mA h cm^{-2}. Long-term cycling of symmetric cells in $ZnSO_4$ without and with the 0.1 m ASA additive at (b) 5 mA cm^{-2} and 5 mA h cm^{-2}, (c) 10 mA cm^{-2} and 2 mA h cm^{-2}, and (d) 35% DOD with thin Zn electrodes. Continuous stripping/plating in symmetric cells with the $ZnSO_4$ electrolytes without and with 0.1 m ASA at (e) 2 mA cm^{-2}, (f) 5 mA cm^{-2}, and (g) 10 mA cm^{-2} and (h) the corresponding DOD. (i) Coulombic efficiencies of Zn plating–stripping in Zn//Cu cells in the two electrolytes. (j) Comparison of cycle life, additive content, current density and areal capacity of 0.1 m ASA with the reported electrolyte additives.

at 99.7% DOD with 2 mA cm^{-2} current density results from the complete consumption of the stripping electrode. The Zn plating-stripping coulombic efficiencies (CEs) are evaluated in Zn//Cu cells (Fig. 1i and S4†). The 0.1-ASA electrolyte delivers a stabilized CE of 99.69% for 700 cycles at 1 mA cm^{-2} and 99.45% for 500 cycles at 10 mA cm^{-2}. By contrast, the cell without ASA fails at the 95th and 18th cycles, respectively. In Fig. 1j and Table S1,† we summarize and compare the cycling stability of Zn anodes with representative electrolyte additives.[24–32] A low additive content of 0.1 m ASA (1.7 wt% relative to H_2O) presents superior effects on Zn under various testing conditions.

The results confirm that the ASA additive, with only 0.1 m concentration in the $ZnSO_4$ electrolyte, is able to significantly enhance the electrochemical performance of the Zn electrode. Considering the multiple functional groups on the ASA molecule, various interactions with the Zn electrode and Zn^{2+} cations in the electrolyte can be formed, through coordination or electrostatic attractions. The ASA adsorption behavior on the Zn surface is first studied. The binding energy of ASA on the Zn (002) surface is calculated by density functional theory (DFT) calculations, which results in a value of −0.283 eV (Fig. 2a). This is stronger than the binding energy of −0.249 eV for water molecule adsorption on Zn. This suggests that the ASA additive tends to replace water and accumulate at the Zn surface. Fig. 2b and c show the charge density difference and 2D contour map of electron density statistics at the interface between Zn and ASA. This reveals the high tendency of electron exchange between the Zn surface and the amino and sulfo sites of ASA, confirming the strong interactions. The interface environment at the Zn electrode is further studied experimentally. The electric double-layer capacitance (EDLC) of the Zn electrode in the two electrolytes is measured by cyclic voltammetry (CV) in the non-faradaic voltage range (Fig. S5†). According to linear fits, Zn exhibits an EDLC of 132 μF cm^{-2} in $ZnSO_4$, whereas a decreased value of 73 μF cm^{-2} is obtained after ASA addition (Fig. 2d). This suggests the replacement of water by ASA in the inner Helmholtz plane layer of Zn and thus the increased distance of the stern layer.[33,34] Fig. 2e shows the contact angles of the two solutions on the Zn electrode. The angles of the $ZnSO_4$ solution change from 91.5° to 89.7° after 120 s. In comparison, the angles of the ASA containing electrolyte decrease from 85.4° to 78.2°. The smaller angles of the latter are attributed to the adsorption of ASA molecules on Zn.[35] The above results illustrate that ASA can replace water molecules in the inner Helmholtz plane layer and construct an ASA-rich interface. Therefore, it is able to significantly affect the electrochemical properties of the Zn electrode despite the low overall concentration of 0.1 m.

The effect of the ASA additive on the solvation structure of Zn^{2+} is investigated by molecular dynamics (MD) simulation (Fig. 2f, g and S6†). In the neat $ZnSO_4$ solution, the inner solvation shell of Zn^{2+} is composed of H_2O and SO_4^{2-} at around 2 Å, with major contribution from the former. Following ASA addition, a Zn^{2+}–N distance of around 2.5 Å is revealed by the

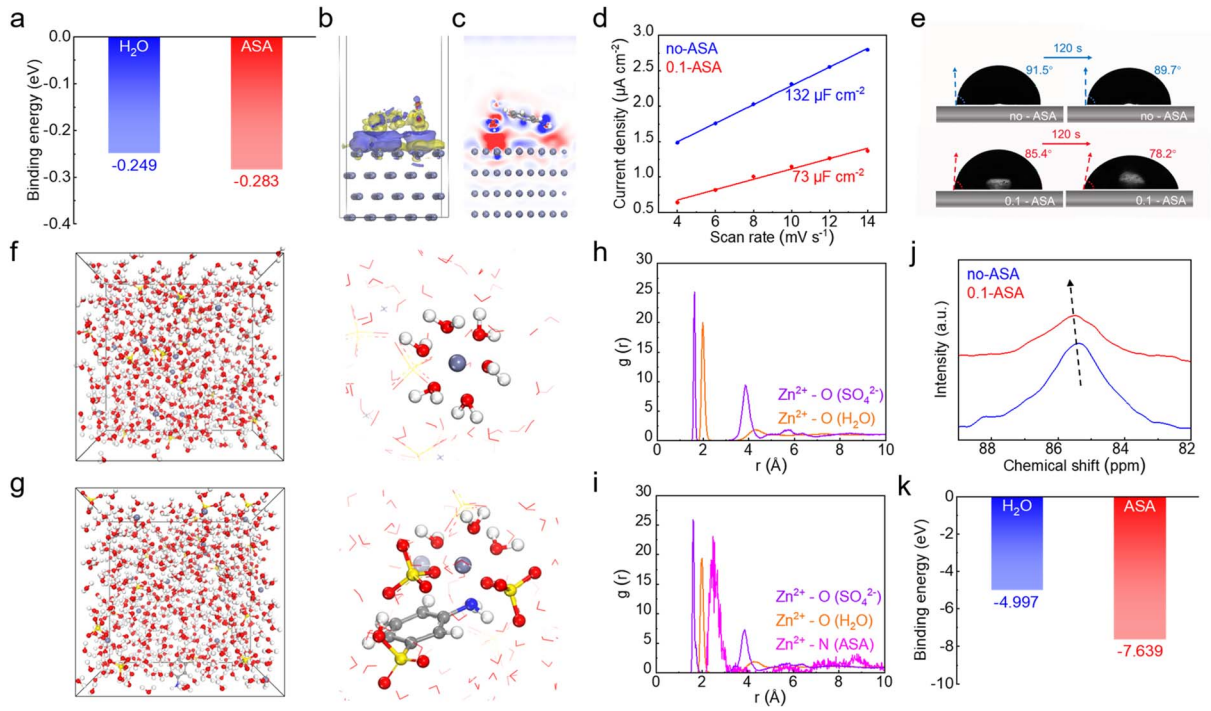

Fig. 2 (a) Adsorption energies of water and ASA molecules on the Zn (002) surface. (b) Charge density difference and (c) sliced 2D contour map reflecting the interactions between ASA and Zn at the interface. (d) Linear fits to calculate the EDLC of Zn in the $ZnSO_4$ electrolytes without and with a 0.1 m ASA additive. (e) Contact angle measurements of Zn foil in the two solutions before and after 120 s. (f) and (g) Snapshots of MD simulation boxes (left), enlarged figures representing Zn^{2+} solvation structures (right), and (h) and (i) RDFs for the $ZnSO_4$ electrolytes (f) and (h) without and (g) and (i) with a 0.1 m ASA additive. (j) ^{67}Zn NMR of the two solutions. (k) Binding energies of Zn^{2+} with water and ASA.

radial distribution function (RDF). This suggests that ASA is also able to enter the inner solvation shell with N as the coordination site. Specifically, a $[Zn(H_2O)_3(ASA)(SO_4)_2]^{2-}$ solvation structure is identified. Fig. 2j compares the ^{67}Zn NMR of $ZnSO_4$ solution without and with a 0.1 m ASA additive. The Zn peak shifts down-field after introducing ASA, which confirms the replacement of some water by ASA in the Zn^{2+} inner solvation sheath.[36] The calculated binding energies of Zn^{2+}–ASA and Zn^{2+}–H_2O suggest the stronger interaction of the former (Fig. 2k), which explains the preferential entrance of ASA in Zn^{2+} inner solvation shells. The mean-squared displacement (MSD) *versus* time plot is obtained to evaluate the diffusion rate of Zn^{2+} in different electrolyte systems. The diffusion coefficient of Zn^{2+}, which is directly proportional to the slope of the MSD *vs.* time curve, increases from 1.37×10^{-6} cm^2 s^{-1} to 1.98×10^{-6} cm^2 s^{-1} with the addition of ASA (Fig. S7†). This facilitated Zn^{2+} transport is also attributed to the regulation of its solvation structures by ASA.

With an ASA-rich Zn–electrolyte interface and preferential entrance of ASA in the Zn^{2+} solvation shell, the electrolyte environment can be illustrated as shown in Fig. 3a. The $[Zn(H_2O)_6]^{2+}$ structure still dominates in the bulk electrolyte considering the low overall ASA concentration, whereas it tends to convert to the ASA containing solvation structure at the ASA-rich interface. This transition is further confirmed by DFT calculations. As shown in Fig. 3b, the relative energy to form the $[Zn(H_2O)_6]^{2+}$ solvation structure is −24.03 eV, which is 22.82 eV higher than that for the formation of $[Zn(H_2O)_3(ASA)(SO_4)_2]^{2-}$. This suggests a thermodynamically spontaneous transformation process,[37] and the latter is favorable at the ASA-rich interface. Fig. 3c compares the LUMO energy levels of $[Zn(H_2O)_6]^{2+}$ and $[Zn(H_2O)_3(ASA)(SO_4)_2]^{2-}$. They exhibit close values of −1.83 eV and −1.69 eV, respectively. Notably, the location of LUMOs represents the sites with a higher tendency of reduction.[38] These orbitals stay on the solvated water molecules in $[Zn(H_2O)_6]^{2+}$, suggesting that they tend to be reduced during Zn deposition in the $ZnSO_4$ electrolyte. This leads to the widely observed HER issue.[39] With the $[Zn(H_2O)_3(ASA)(SO_4)_2]^{2-}$ structure, on the other hand, the LUMOs dominate on ASA instead of water. This would not only enhance the HER resistivity of solvated water, but also generate an SEI after ASA decomposition on Zn, which further regulates the electrochemical performance of the Zn electrode.

The surface composition of electro-deposited Zn (15 mA h cm^{-2}) from the 0.1-ASA electrolyte is studied by X-ray photoelectron spectroscopy (XPS, Fig. 3d). The components

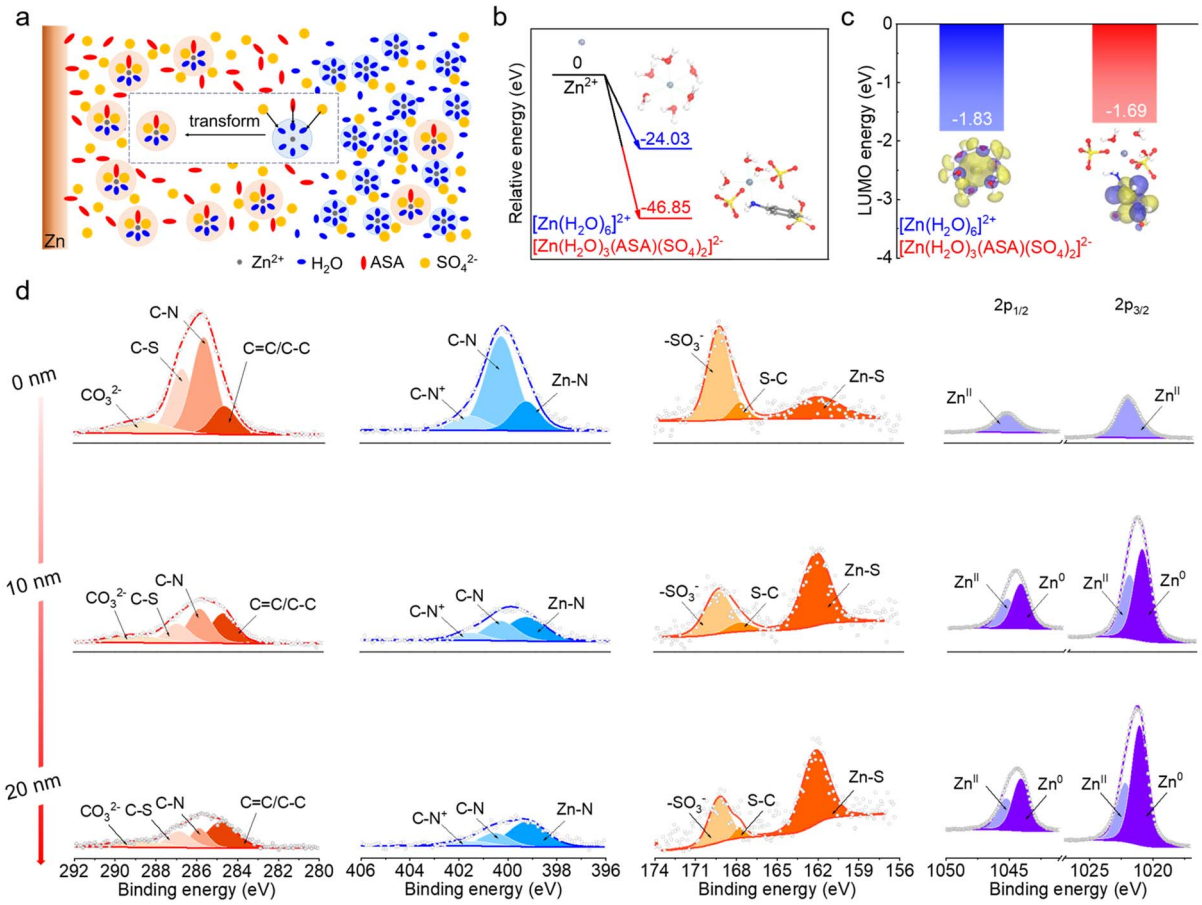

Fig. 3 (a) Schematic illustrations of Zn^{2+} solvation structures in the bulk electrolyte and at the interface. (b) The relative energies for the formation of $[Zn(H_2O)_6]^{2+}$ and $[Zn(H_2O)_3(ASA)(SO_4)_2]^{2-}$. (c) The LUMO energy levels and orbitals of $[Zn(H_2O)_6]^{2+}$ and $[Zn(H_2O)_3(ASA)(SO_4)_2]^{2-}$. (d) The C 1s, N 1s, S 2p and Zn 2p XPS with different sputtering depths of the electro-deposited Zn from the 0.1-ASA electrolyte.

derived from ASA are evidenced in the C 1s, N 1s and S 2p spectra. In the spectra of the un-sputtered electrode, which reflects the top surface environment, C–N, C–S, CO_3^{2-}, Zn–N, –SO_3^- and Zn–S peaks are revealed. Together with Zn^{II} peaks in the Zn 2p spectrum, it suggests that the outer SEI is composed of organic species as well as $ZnCO_3$ and ZnS inorganic components. The absence of Zn^0 signals suggests complete coverage on the Zn electrode. As the Ar^+ sputtering depth increases, most C, N and S peaks diminish except for the increase in the ZnS peak. This demonstrates that the inner SEI is mainly composed of ZnS, which is beneficial for Zn^{2+} transport.[40] The increase of Zn^0 peaks in the Zn 2p spectra results from the detection of underlying Zn metal after gradual removal of SEI coverage. The analysis suggests that the top surface of the SEI mainly contains $ZnCO_3$, ZnS and organic species, whereas ZnS dominates in the inner SEI. This gradient SEI layer not only provides excellent protection for the underlying Zn to avoid direct contact with electrolyte and ensure good mechanical strength, but also provides Zn^{2+} diffusion paths and homogenizes Zn^{2+} flux.

The effects of the ASA additive on the stability and deposition behavior of Zn are studied. Fig. 4a shows the X-ray diffraction (XRD) patterns of Zn foil after soaking in the $ZnSO_4$ solutions without and with an ASA additive for 24 h. From the neat $ZnSO_4$ solution, an extra diffraction peak of $Zn_4(OH)_6SO_4\cdot H_2O$ is observed. It is attributed to the chemical reaction between Zn and the mildly acidic $ZnSO_4$ solution, which causes local pH increase and the precipitation of basic zinc salts. A corroded Zn surface is also observed in the scanning electron microscopy (SEM) image (Fig. 4b). In comparison, no extra diffractions are found on the Zn electrode soaked in the ASA containing electrolyte, and the surface remains flat. This suggests the enhanced chemical stability of the Zn electrode with the help of ASA. Fig. 4c compares the Tafel plots of the Zn electrode in the two electrolytes. With the addition of ASA, the corrosion current density significantly decreases from 643 μA cm^{-2} to 8 μA cm^{-2}, which suggests much suppressed corrosion on the Zn electrode.[41,42] The above promoted chemical and electrochemical stabilities of the Zn electrode are attributed to the replacement of interface water by ASA and the regulated LUMOs of solvated structures.

Fig. 4d compares the chronoamperometry (CA) curves of the Zn electrode in the two electrolytes at −150 mV *vs.* Zn. In the neat $ZnSO_4$ electrolyte, the current density continuously increases for more than 5 min. This corresponds to the rapid formation of active sites that lead to uneven Zn deposition. In comparison, the current density exhibits negligible change after the initial 3 s in the 0.1-ASA electrolyte, which suggests the reduced surface activity and steady deposition of Zn.[43–45] The electrochemical deposition is further carried out by the galvanostatic process at 15 mA cm^{-2} for 1 h on a Cu substrate. As shown in Fig. 4e, loosely packed particles are found on the surface from the $ZnSO_4$ electrolyte, whereas the one from 0.1-ASA exhibits densely packed plates. The uniform deposition of the latter is realized by the non-corroded surface to start with as well as the homogeneous Zn^{2+} flux, which are provided by the ASA-rich interface, regulated Zn^{2+} solvation structures and stable SEI. They overall ensure the extended DOD and cycle life of the Zn electrode in the 0.1-ASA electrolyte.

To investigate the feasibility of the 0.1-ASA electrolyte for cathode materials, it is applied to a $V_6O_{13}\cdot H_2O$ cathode (Fig. S8†) in zinc cells. Fig. 5a shows the cyclic voltammogram at 0.5 mV s^{-1}, which exhibits stable redox peaks after several cycles. The electrochemical performance of the $V_6O_{13}\cdot H_2O$ cathode is further compared in the two electrolytes by galvanostatic charge–discharge (Fig. 5b and S9†). In the $ZnSO_4$ electrolyte, the cathode delivers 374 mA h g^{-1} capacity at 0.5 A g^{-1} and only 209 mA h g^{-1}

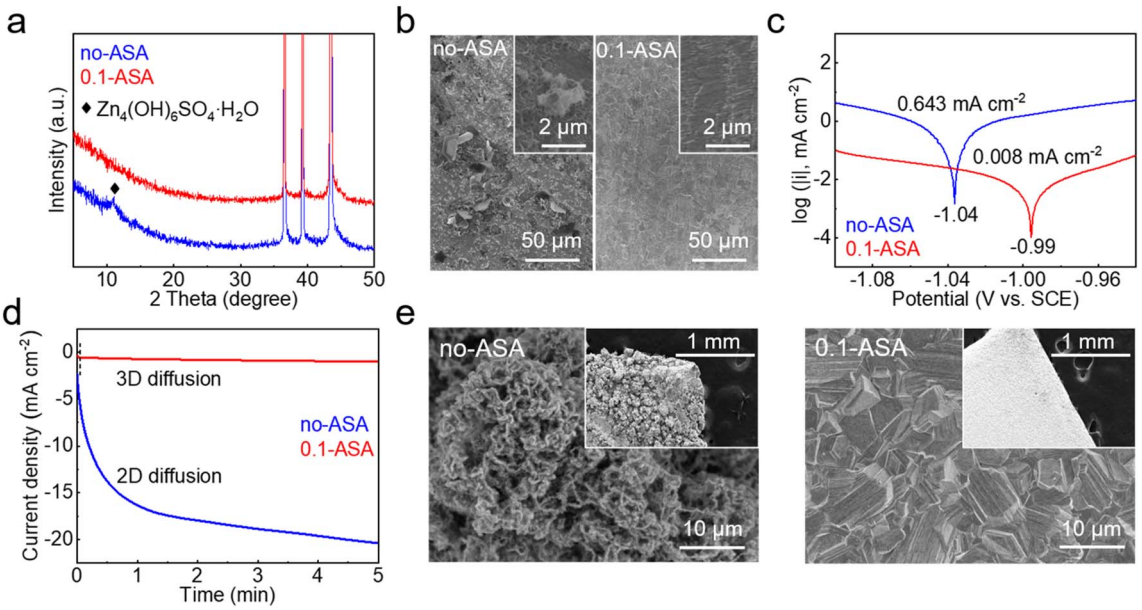

Fig. 4 (a) XRD patterns and (b) SEM images of Zn after soaking in the two solutions for 24 h. (c) Tafel plots and (d) CA curves at −150 mV *vs.* Zn constant potential in the two electrolytes. (e) SEM images of the electro-deposited Zn (at 10 mA cm^{-2} for 1.5 h) in the two electrolytes.

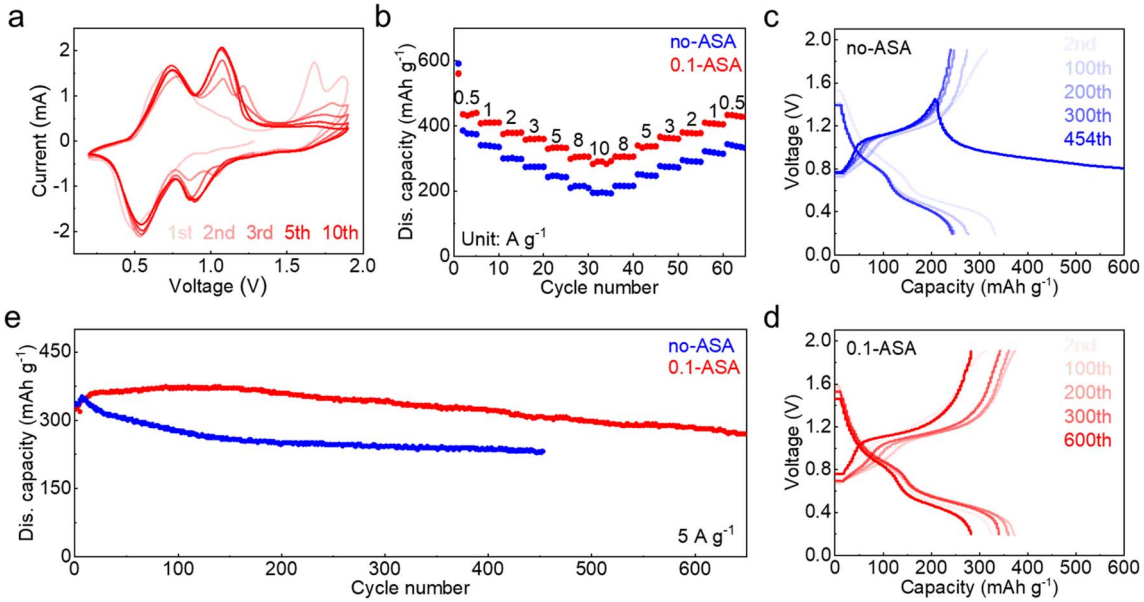

Fig. 5 Electrochemical performance of the $V_6O_{13}\cdot H_2O$ cathode in the $ZnSO_4$ electrolyte without and with a 0.1 m ASA additive. (a) CV curves in 0.1-ASA. (b) Rate performance in the two electrolytes. Charge–discharge curves at different cycles in (c) $ZnSO_4$ and (d) 0.1-ASA, and (e) the capacity evolution at 5 A g^{-1}.

capacity is left at 10 A g^{-1}. A poor capacity preservation of 333 mA h g^{-1} is obtained when the current density returns to 0.5 A g^{-1}. With the addition of 0.1 m ASA, in contrast, the cathode realizes higher capacity and better rate performance. It delivers a capacity of 440 mA h g^{-1} at 0.5 A g^{-1}, and 291 mA h g^{-1} capacity is obtained with the increase of current density to 10 A g^{-1}. A good capacity of 428 mA h g^{-1} is also preserved when the current density returns to 0.5 A g^{-1}. Electrochemical impedance spectroscopy (EIS) reveals a smaller charge-transfer resistance in the 0.1-ASA electrolyte (Fig. S10†), which suggests enhanced electrochemical kinetics and ensures better rate performance.[46] Long-term cycling is carried out at 5 A g^{-1}. The ASA free cell suffers a soft short circuit at the 454th cycle, whereas the cathode maintains 270 mA h g^{-1} capacity after 650 cycles with the help of ASA (Fig. 5c–e). The results confirm that the ASA electrolyte additive not only effectively enhances the cycling stability of the Zn electrode but also ensures the desired electrochemical performance of full cells.

Conclusions

In conclusion, we present a low concentration electrolyte additive, 0.1 m ASA, for aqueous Zn batteries. Thanks to its preferential adsorption on the Zn surface over water, a locally ASA-rich environment is created despite the low overall concentration. The water-rich Zn^{2+} solvation sheath in the bulk electrolyte spontaneously transforms into an ASA-participated structure at the interface, which shifts the LUMOs from solvated water to solvated ASA. This not only suppresses the HER but also generates a gradient SEI composed of inner ZnS covered with organic–inorganic mixed components. With the help of the ASA additive, the highest DOD for Zn stripping in symmetric cells increases from 11.4% to 99.7%, and the cycle life of repeated stripping/plating extends from 110 h to 1100 h at 2 mA cm^{-2}. The ASA additive also enables a longer cycle life for the $V_6O_{13}\cdot H_2O$ cathode in aqueous Zn batteries. Our results confirm that interface regulation is an efficient way to promote the electrochemical behavior of the Zn anode, which allows the reduction of additive concentration to retain the aqueous nature of bulk electrolytes. This would put forward promising approaches for high-safety aqueous Zn batteries.

Data availability

Data are available from the authors on reasonable request.

Author contributions

K. W., Q. L. and X. S. conceived and designed this work. K. W. and Q. L. carried out the synthesis, electrochemical measurements and computational calculations. All authors participated in the analysis of the data and discussed and revised the manuscript.

Conflicts of interest

There are no conflicts to declare.

Acknowledgements

This work was supported by the National Natural Science Foundation of China (52174276 and 51974070), the Fundamental Research Funds for the Central Universities (N2105001 and N232410019), and the 111 Project (B16009). Special thanks are due to the instrumental analysis from Analytical and Testing Center, Northeastern University.

References

1 Z. Yi, G. Chen, F. Hou, L. Wang and J. Liang, Strategies for the Stabilization of Zn Metal Anodes for Zn-Ion Batteries, *Adv. Energy Mater.*, 2021, **11**, 2003065.

2 Y. Chai, X. Xie, Z. He, G. Guo, P. Wang, Z. Xing, B. Lu, S. Liang, Y. Tang and J. Zhou, A smelting–rolling strategy for ZnIn bulk phase alloy anodes, *Chem. Sci.*, 2022, **13**, 11656–11665.

3 N. Dong, F. Zhang and H. Pan, Towards the practical application of Zn metal anodes for mild aqueous rechargeable Zn batteries, *Chem. Sci.*, 2022, **13**, 8243–8252.

4 G. Ma, L. Miao, W. Yuan, K. Qiu, M. Liu, X. Nie, Y. Dong, N. Zhang and F. Cheng, Non-flammable, dilute, and hydrous organic electrolytes for reversible Zn batteries, *Chem. Sci.*, 2022, **13**, 11320–11329.

5 J. Shin, J. Lee, Y. Park and J. W. Choi, Aqueous zinc ion batteries: focus on zinc metal anodes, *Chem. Sci.*, 2020, **11**, 2028–2044.

6 L. Ma, S. Chen, N. Li, Z. Liu, Z. Tang, J. A. Zapien, S. Chen, J. Fan and C. Zhi, Hydrogen-Free and Dendrite-Free All Solid-State Zn-Ion Batteries, *Adv. Mater.*, 2020, **32**, 1908121.

7 H.-F. Wang, C. Tang and Q. Zhang, A review of precious-metal-free bifunctional oxygen electrocatalysts: rational design and applications in Zn-air batteries, *Adv. Funct. Mater.*, 2018, **28**, 1803329.

8 B. Tang, L. Shan, S. Liang and J. Zhou, Issues and opportunities facing aqueous zinc-ion batteries, *Energy Environ. Sci.*, 2019, **12**, 3288.

9 L. E. Blanc, D. Kundu and L. F. Nazar, Scientific Challenges for the Implementation of Zn-Ion Batteries, *Joule*, 2020, **4**, 771–799.

10 L. Geng, J. Meng, X. Wang, C. Han, K. Han, Z. Xiao, M. Huang, P. Xu, L. Zhang, L. Zhou and L. Mai, Eutectic Electrolyte with Unique Solvation Structure for High Performance Zinc-Ion Batteries, *Angew. Chem., Int. Ed.*, 2022, **61**, e202206717.

11 Z. Hou, T. Zhang, X. Liu, Z. Xu, J. Liu, W. Zhou, Y. Qian, H. J. Fan, D. Chao and D. Zhao, A solid-to-solid metallic conversion electrochemistry toward 91% zinc utilization for sustainable aqueous batteries, *Sci. Adv.*, 2022, **8**, eabp8960.

12 J. Liu, W. Zhou, R. Zhao, Z. Yang, W. Li, D. Chao, S.-Z. Qiao and D. Zhao, Sulfur-Based Aqueous Batteries: Electrochemistry and Strategies, *J. Am. Chem. Soc.*, 2021, **143**, 15475–15489.

13 N. Liu, X. Wu, L. Fan, S. Gong, Z. Guo, A. Chen, C. Zhao, Y. Mao, N. Zhang and K. Sun, Intercalation Pseudocapacitive Zn^{2+} Storage with Hydrated Vanadium Dioxide toward Ultrahigh Rate Performance, *Adv. Mater.*, 2020, **32**, 1908420.

14 A. Chen, C. Zhao, J. Gao, Z. Guo, X. Lu, J. Zhang, Z. Liu, M. Wang, N. Liu, L. Fan, Y. Zhang and N. Zhang, Multifunctional SEI-like structure coating stabilizing Zn anodes at a large current and capacity, *Energy Environ. Sci.*, 2023, **16**, 275–284.

15 Y. Shang, P. Kumar, T. Musso, U. Mittal, Q. Du, X. Liang and D. Kundu, Long-Life Zn Anode Enabled by Low Volume Concentration of a Benign Electrolyte Additive, *Adv. Funct. Mater.*, 2022, **32**, 2200606.

16 W. Sun, F. Wang, B. Zhang, M. Zhang, V. Küpers, X. Ji, C. Theile, P. Bieker, K. Xu, C. Wang and M. Winter, A rechargeable zinc-air battery based on zinc peroxide chemistry, *Science*, 2021, **371**, 46–51.

17 K. Wang, T. Qiu, L. Lin, X.-X. Liu and X. Sun, A low fraction electrolyte additive as interphase stabilizer for Zn electrode in aqueous batteries, *Energy Storage Mater.*, 2023, **54**, 366–373.

18 Z. Yang, B. Wang, Y. Chen, W. Zhou, H. Li, R. Zhao, X. Li, T. Zhang, F. Bu, Z. Zhao, W. Li, D. Chao and D. Zhao, Activating sulfur oxidation reaction via six-electron redox mesocrystal NiS_2 for sulfur-based aqueous batteries, *Natl. Sci. Rev.*, 2022, **10**, nwac268.

19 Y. Li, Y. Wang, Y. Xu, W. Tian, J. Wang, L. Cheng, H. Yue, R. Ji, Q. Zhu, H. Yuan and H. Wang, Dynamic biomolecular "mask" stabilizes Zn anode, *Small*, 2022, **18**, 2202214.

20 J. Wang, Y. Yang, Y. Zhang, Y. Li, R. Sun, Z. Wang and H. Wang, Strategies towards the challenges of zinc metal anode in rechargeable aqueous zinc ion batteries, *Energy Storage Mater.*, 2021, **35**, 19.

21 Y. Dong, L. Miao, G. Ma, S. Di, Y. Wang, L. Wang, J. Xu and N. Zhang, Non-concentrated aqueous electrolytes with organic solvent additives for stable zinc batteries, *Chem. Sci.*, 2021, **12**, 5843.

22 G. Q. Ma, L. C. Miao, Y. Dong, W. T. Yuan, X. Y. Nie, S. L. Di, Y. Y. Wang, L. B. Wang and N. Zhang, Reshaping the electrolyte structure and interphase chemistry for stable aqueous zinc batteries, *Energy Storage Mater.*, 2022, **47**, 2405–8297.

23 F. W. Ming, Y. P. Zhu, G. Huang, A. H. Emwas, H. F. Liang, Y. Cui and H. N. Alshareef, Co-Solvent Electrolyte Engineering for Stable Anode-Free Zinc Metal Batteries, *J. Am. Chem. Soc.*, 2022, **144**(16), 7160–7170.

24 Y. Zhang, M. Zhu, K. Wu, F. Yu, G. Wang, G. Xu, M. Wu, H. K. Liu, S. X. Dou and C. Wu, An in-depth insight of a highly reversible and dendrite-free Zn metal anode in an hybrid electrolyte, *J. Mater. Chem. A*, 2021, **9**, 4253–4261.

25 N. Chang, T. Li, R. Li, S. Wang, Y. Yin, H. Zhang and X. Li, An aqueous hybrid electrolyte for low-temperature zinc-based energy storage devices, *Energy Environ. Sci.*, 2020, **13**, 3527–3535.

26 F. Yang, J. A. Yuwono, J. Hao, J. Long, L. Yuan, Y. Wang, S. Liu, Y. Fan, S. Zhao, K. Davey and Z. Guo, Understanding H_2 Evolution Electrochemistry to Minimize Solvated Water Impact on Zinc-Anode Performance, *Adv. Mater.*, 2022, **34**, 2206754.

27 L. Cao, D. Li, E. Hu, J. Xu, T. Deng, L. Ma, Y. Wang, X. Q. Yang and C. Wang, Solvation Structure Design for Aqueous Zn Metal Batteries, *J. Am. Chem. Soc.*, 2020, **142**, 21404–21409.

28 R. Yao, L. Qian, Y. Sui, G. Zhao, R. Guo, S. Hu, P. Liu, H. Zhu, F. Wang, C. Zhi and C. Yang, A Versatile Cation Additive

Enabled Highly Reversible Zinc Metal Anode, *Adv. Energy Mater.*, 2022, **12**, 2102780.

29 Z. Liu, R. Wang, Q. Ma, J. Wan, S. Zhang, L. Zhang, H. Li, Q. Luo, J. Wu, T. Zhou, J. Mao, L. Zhang, C. Zhang and Z. Guo, A Dual-Functional Organic Electrolyte Additive with Regulating Suitable Overpotential for Building Highly Reversible Aqueous Zinc Ion Batteries, *Adv. Funct. Mater.*, 2023, 2214538.

30 Z. Hou, H. Tan, Y. Gao, M. Li, Z. Lu and B. Zhang, Tailoring desolvation kinetics enables stable zinc metal anodes, *J. Mater. Chem. A*, 2020, **8**, 19367–19374.

31 T. C. Li, Y. Lim, X. L. Li, S. Luo, C. Lin, D. Fang, S. Xia, Y. Wang and H. Y. Yang, A Universal Additive Strategy to Reshape Electrolyte Solvation Structure toward Reversible Zn Storage, *Adv. Energy Mater.*, 2022, **12**, 2103231.

32 X.-X. Guo, Z.-Y. Zhang, J.-W. Li, N.-J. Luo, G.-L. Chai, T. S. Miller, F.-L. Lai, P. Shearing, D. J. L. Brett, D.-L. Han, Z. Weng, G.-J. He and I. P. Parkin, Alleviation of Dendrite Formation on Zinc Anodes via Electrolyte Additives, *ACS Energy Letters*, 2021, **6**(2), 395–403.

33 L. Miao, R. Wang, S. Di, Z. Qian, L. Zhang, W. Xin, M. Liu, Z. Zhu, S. Chu, Y. Du and N. Zhang, Aqueous Electrolytes with Hydrophobic Organic Cosolvents for Stabilizing Zinc Metal Anodes, *ACS Nano*, 2022, **16**, 9667–9678.

34 L. Zhang, L. Miao, W. Xin, H. Peng, Z. Yan and Z. Zhu, Engineering zincophilic sites on Zn surface via plant extract additives for dendrite-free Zn anode, *Energy Storage Mater.*, 2022, **44**, 408–415.

35 Q. Gou, H. Luo, Q. Zhang, J. Deng, R. Zhao, O. Odunmbaku, L. Wang, L. Li, Y. Zheng, J. Li, D. Chao and M. Li, Electrolyte Regulation of Bio-Inspired Zincophilic Additive toward High-Performance Dendrite-Free Aqueous Zinc-Ion Batteries, *Small*, 2023, **19**, 2207502.

36 L. Cao, D. Li, E. Hu, J. Xu, T. Deng, L. Ma, Y. Wang, X.-Q. Yang and C. Wang, Solvation Structure Design for Aqueous Zn Metal Batteries, *J. Am. Chem. Soc.*, 2020, **142**(51), 21404–21409.

37 J. Xu, W.-L. Lv, W. Yang, Y. Jin, Q.-Z. Jin, B. Sun, Z.-L. Zhang, T.-Y. Wang, L.-F. Zheng, X.-L. Shi, B. Sun and G.-X. Wang, In Situ Construction of Protective Films on Zn Metal Anodes via Natural Protein Additives Enabling High-Performance Zinc Ion Batteries, *ACS Nano*, 2022, **16**(7), 11392–11404.

38 D. Wang, D. Lv, H. Peng, C. Wang, H. Liu, J. Yang and Y. Qian, Solvation Modulation Enhances Anion-Derived Solid Electrolyte Interphase for Deep Cycling of Aqueous Zinc Metal Batteries, *Angew. Chem., Int. Ed.*, 2023, **62**, e202310290.

39 K. Wang, T. Qiu, L. Lin, F. Liu, J. Zhu, X.-X. Liu and X. Sun, Interphase solvation regulation stabilizing the Zn metal anode in aqueous Zn batteries, *Chem. Sci.*, 2023, **14**, 8076–8083.

40 J. Hao, B. Li, X. Li, X. Zeng, S. Zhang, F. Yang, S. Liu, D. Li, C. Wu and Z. Guo, An In-Depth Study of Zn Metal Surface Chemistry for Advanced Aqueous Zn-Ion Batteries, *Adv. Mater.*, 2020, **32**, 2003021.

41 T.-Y. Zhou, Y.-L. Mu, L. Chen, D.-X. Li, W. Liu, C.-K. Yang, S.-B. Zhang, Q. Wang, P. Jiang, G.-L. Ge and H.-H. Zhou, Toward stable zinc aqueous rechargeable batteries by anode morphology modulation via polyaspartic acid additive, *Energy Storage Mater.*, 2022, **45**, 2405–8297.

42 M. Zhang, H. Hua, P. Dai, Z. He, L. Han, P. Tang, J. Yang, P. Lin, Y. Zhang, D. Zhan, J. Chen, Y. Qiao, C. C. Li, J. Zhao and Y. Yang, Dynamically Interfacial pH-Buffering Effect Enabled by N-Methylimidazole Molecules as Spontaneous Proton Pumps toward Highly Reversible Zinc-Metal Anodes, *Adv. Mater.*, 2023, **35**, 2208630.

43 W. Zhang, Y. Dai, R. Chen, Z. Xu, J. Li, W. Zong, H. Li, Z. Li, Z. Zhang, J. Zhu, F. Guo, X. Gao, Z. Du, J. Chen, T. Wang, G. He and I. P. Parkin, Highly Reversible Zinc Metal Anode in a Dilute Aqueous Electrolyte Enabled by a pH Buffer Additive, *Angew. Chem.*, 2023, **135**, e202212695.

44 Y.-M. Chen, F.-C. Gong, W.-J. Deng, H. Zhang and X.-L. Wang, Dual-function electrolyte additive enabling simultaneous electrode interphase and coordination environment regulation for zinc-ion batteries, *Energy Storage Mater.*, 2023, **58**, 2405–8297.

45 J. Yang, B. Yin, S. Zhang, Y. Sun, J. Li, D. Su and T. Ma, Macromolecules Promoting Robust Zinc Anode by Synergistic Coordination Effect and Charge Redistribution, *Small*, 2023, 2304913.

46 Y. Li, X. Peng, X. Li, H. Duan, S. Xie, L. Dong and F. Kang, Functional Ultrathin Separators Proactively Stabilizing Zinc Anodes for Zinc-Based Energy Storage, *Adv. Mater.*, 2023, **35**, 2300019.